Proceedings of ASME Turbo Expo 2024
Turbomachinery Technical Conference and Exposition
GT2024
June 24-28, 2024, London, United Kingdom

GT2024-122599

EVALUATION OF MECHANICAL PROPERTIES OF ADDITIVELY MANUFACTURED BEAMS WITH LATTICE STRUCTURES

Inci Pir
Faculty of Mechanical Engineering, Istanbul Technical University
Istanbul, Turkey

Serhat Arda Sahin
Faculty of Mechanical Engineering, Istanbul Technical University
Istanbul, Turkey

Mertol Tufekci
Center for Engineering Research, University of Hertfordshire
Hertfordshire, United Kingdom

School of Physics, Engineering and Computer Science, University of Hertfordshire, Hatfield, Hertfordshire AL10 9AB, UK

Ekrem Tufekci
Faculty of Mechanical Engineering, Istanbul Technical University
Istanbul, Turkey

ABSTRACT

The use of lattice structurses is becoming more common day by day. Limitations such as being expensive and time-consuming have led to a search for new solutions in the industry. In light of these limitations, the widespread use of 3D printing technology methods is evaluated. 3D printing technology has advantages in terms of design flexibility, quick prototyping, lightness and the ability to produce complex shapes. 3D printing is used to systematically investigate different geometries in line with the requirements of sustainable product development, leading to the production of auxiliary structures that are both strong and lightweight. This research investigates the mechanical properties of various lattice structures that were previously modelled and analysed through analytical methods in the literature. The samples with five different auxetic structures are manufactured using the Fused Deposition Modelling (FDM) 3D printing technique, with Acrylonitrile Butadiene Styrene (ABS) as the selected material. The manufactured samples are subjected to a three-point bending test to assess their mechanical characteristics, including the flexural modulus, flexural strength, and elongation at break, and the effect of the in-plane geometry on the mechanical behaviour is evaluated.

Keywords: Lattice structures, 3D Printing, Beam, Three-Point Bending Test

NOMENCLATURE

Letters and Symbols

FDM	Fused Deposition Modelling
ABS	Acrylonitrile Butadiene Styrene
CAD	Computer-Aided Design
AUX	Auxetic
ASTM	American Society for Testing and Materials
E	Elasticity Modulus
F	Force
l	Span
MPa	Megapascal
w	Deflection
b	Width
h	Height

1. INTRODUCTION

Metamaterials, designed with micro-structures to achieve macro-scale properties/behaviours under certain conditions, are becoming more commonly used due to the progress in additive manufacturing [1,2]. Lattices, which are a specific type of metamaterial created by tessellating a periodic unit cell, have captured significant research attention. However, they are difficult to manufacture using traditional manufacturing techniques/methods structures [3–6]. These structures are often inspired by natural formations such as hexagonal lattices, which are known for their stiffness, toughness, and energy absorption and are investigated for their potential to achieve an optimal stiffness-to-weight ratio in engineering applications [7,8]. However, the absolute stiffness and strength, crucial for applications that require specific deformation characteristics, also remain a critical focus of research [9]. Recent studies have expanded the scope of metamaterials, exploring novel classes of 2D structural metamaterials with curved elements in their unit

cells to enhance mechanical properties, introducing significant application flexibility to lattices [10–12]. This flexibility is quite beneficial for applications ranging from bioengineering to stretchable electronics and impact absorbers [13–17].

The geometric properties of the lattice elements are instrumental in dictating their overall behaviour [18,19]. The unit cell approach, which is particularly common in studies of honeycomb materials, has been crucial in determining the equivalent material behaviour of entire lattices. It is widely used in the aerospace industry due to its specific stiffness and low density [9,20–23]. Efforts in research have concentrated on both regular and irregular hexagonal lattice materials to calculate their equivalent elastic moduli, aiming to enhance structural stiffness [24]. Alongside geometry, tailoring the material for lattice structures is another important focus of research, especially when additive manufacturing is involved in the manufacturing process, as the material properties are significantly affected by the thermomechanical processes during manufacturing [25–28].

Fused Deposition Modelling (FDM), used to create the lattice structures investigated in this study, is a technique that is one of the most commonly used processes in the manufacture of lattice structures. FDM works by passing a thermoplastic filament through a heated nozzle, effectively depositing the molten material in a pre-defined pattern on the build platform [29,30]. As each layer solidifies, the build platform descends, allowing the addition of subsequent layers. Temperature control of the nozzle and heatsink is essential, with cooling fans preventing heat build up that could disrupt the extrusion process. In FDM, the deposition trajectory is controlled by the geometry defined in the slicing software. This significantly influences the mechanical properties of the structures alongside other key printing parameters such as temperature, layer height, etc. [31,32]. Despite these measures, the regulation of the printed structure's cooling process largely remains unregulated.

The process of selecting infill patterns in Fused Deposition Modelling (FDM) is crucial in generating 3D printed lattice beams and is determined by the slicing software, which provides a variety of pattern options, including concentric, honeycomb and rectilinear [33]. These infill patterns significantly influence the weight, strength, stiffness, and overall printing time of the lattice structures. Previous studies have shown that rectilinear patterns with greater infill density produce higher tensile strength and lighter structures compared to honeycomb patterns [34]. However, honeycomb patterns exhibit superior tensile strength at lower infill densities, although this advantage decreases as the infill density approaches 100%. The rectilinear pattern requires a 90-degree shift in layer orientation with each new layer, which leads to bridging over gaps and void formation. The void formation decreases with greater infill density. Additionally, applying compressive forces along the z-axis can improve layer adhesion and close small voids, potentially enhancing the mechanical properties of the structures. Motivated by these findings, this study aims to investigate the mechanical behaviour of different infill lattice geometries and explore how these configurations impact the mechanical behaviour and performance of 3D printed materials.

In this study, lattice structures are employed to enhance mechanical strength in specific directions and reduce the structure's overall weight by removing materials from where there would be less contribution to the stiffness and strength under a certain loading. The mechanical properties of these structures vary depending on the geometric and topological configurations of the lattices in the systems where they are used, as well as depending on the material that the structures are made of and the technique selected for their manufacturing. The numerical modelling of lattice structures typically relies on the principles of the Timoshenko beam theory and Bloch's theorem. Lightweight lattice structures have the potential to be used in rotating components as they are mechanically optimised as foams [28,35,36]. Commonly employed lattice structure types in the literature are hexagonal (honeycomb), rhombus, and tetragonal lattice structures. They can be helpful in protective equipment that can reduce the risk of failure and/or absorb impacts. As another use, athletic shoe soles can be made from lattice structures to increase shock-absorbing properties. Studies are ongoing on optimising these materials and structures for broader applications and providing more significant advantages. In this research, a detailed investigation is undertaken on the mechanical properties of various lattice structures, which were previously modelled and analysed through analytical methods in the literature [10,37–39]. For the purpose of testing, specimen models are carefully generated through computer-aided design software, conforming to various lattice geometrical configurations. These digitally prepared test samples are then manufactured via a 3D printing technique called FDM, employing Acrylonitrile Butadiene Styrene (ABS) as the chosen material. Upon manufacturing, the resulting samples are subject to three-point bending tests, focusing on both mechanical and viscoelastic characteristics. Properties such as the flexural modulus, flexural strength, and elongation at break are mainly assessed. This comparison is made against reference samples that maintain consistent infill ratios and filament orientations for a standard tetragonal lattice framework. This helps to highlight the variations in mechanical performance influenced by the diversity of lattice geometries under consideration.

2. MATERIALS AND METHODS

The in-plane behaviour of laminated composites is profoundly influenced by the core structure. In this context, an examination is conducted on six distinct core topologies. The fundamental aim of this study is to identify the deformation patterns of cells and investigate their impact on the performance of sandwich panels. Consequently, a 2D topology is chosen, with volume fractions are aimed as 25% and sample wall thicknesses established at 0.8 mm. Five diverse cellular structures are selected to ensure uniform unit cell dimensions. This approach facilitates a more direct observation of the varied unit cell deformation patterns. The cross-section images of the internal structures designed cellular structures are shown in Figure 1. In Figure 1, where the coordinate axes are given, the 3D printer nozzle moved in the x-z plane direction and the y axis represents the height of the printed samples.

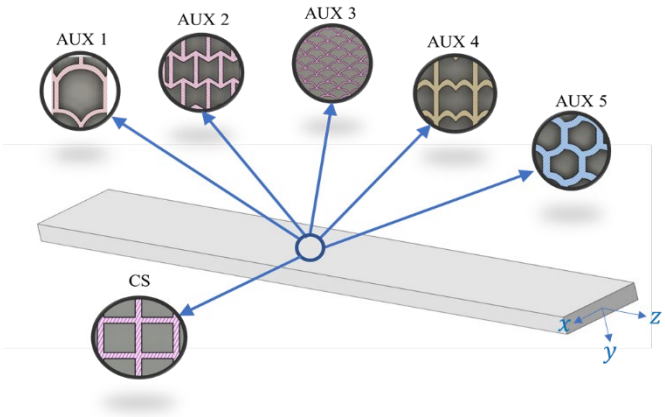

FIGURE 1: CROSS-SECTION OF THE DESIGNED SAMPLES, AUX 1, 2, 3, 4 AND 5 RESPECTIVELY

Careful consideration is given to the internal structures, opting for auxetic geometries to create five distinct three-point bending test samples. Additionally, a reference sample is designed with a non-auxetic tetragonal geometry for comparative purposes in the three-point bending test. The decision to print the samples at a 45-degree position is deliberate, aiming to align the filaments in a straight direction at 0 degrees for optimal performance during the test.

Dimensional details and unit cell dimensions of specimens are detailed in Figure 2. Additionally, hatched areas are also seen in this figure. These hatched areas also provide information about the printing direction of samples. In the printing process of samples, one layer is printed in the direction of these scans, while the following one is printed perpendicular to that.

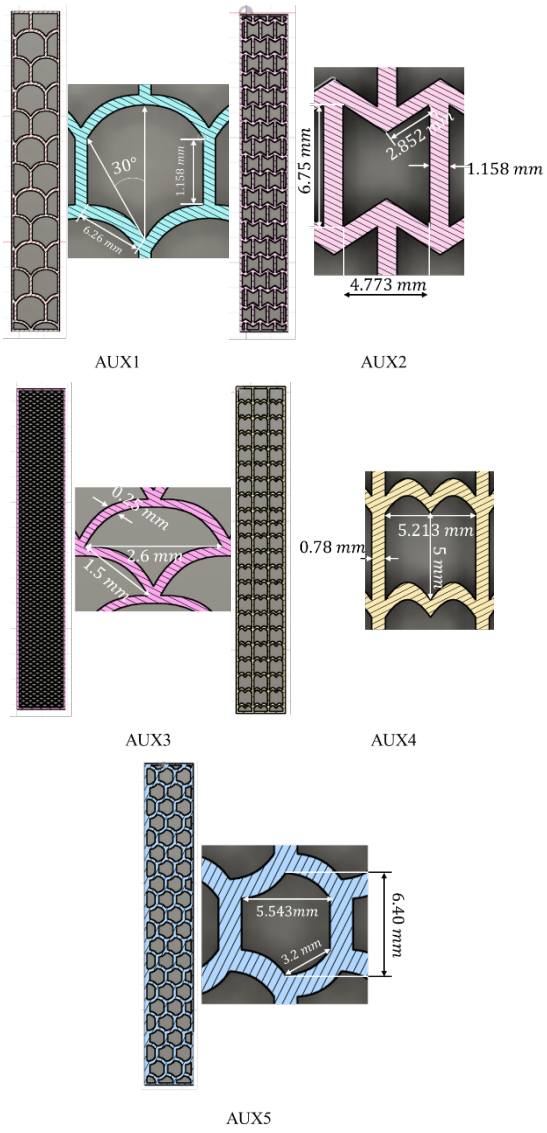

FIGURE 2: DETAILED VISUALISATION OF THE DESIGNED SAMPLES, AUX 1, 2, 3, 4 AND 5 RESPECTIVELY

Specimen models conforming to various lattice geometrical configurations are generated through computer-aided design software for testing purposes considering the ASTM D790 standard, which dedicates the standard test method for flexural properties of unreinforced and reinforced plastics and electrical insulating materials, is used for the testing procedure. The schematic view of the printed samples is given in Figure 3, and dimensions are given in mm.

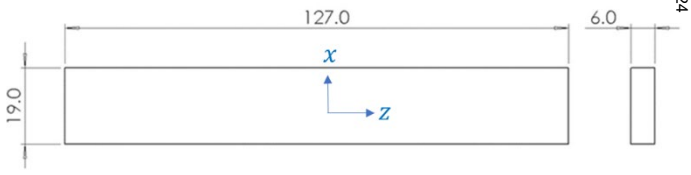

FIGURE 3: THE SCHEMATIC VIEW OF THE PRINTED SAMPLES

2.1 Manufacturing of Samples

The ZAXE Z3 model printer is selected for its suitability for the task, and the ZAXE ABS 1.75mm filament is chosen as the printing material. Key parameters during the 3D printing process included a feed rate of 15 mm/s, a nozzle temperature of 225 °C, and a print bed temperature of 60°C. The printed samples boasted 20% and 30% infill densities, and a consistent wall thickness of 0.8 mm is maintained.

The selection of the 45-degree position, along with the filament alignment, aimed to enhance the structural integrity of the samples. This approach is considered essential for achieving optimal performance and reliable results.

2.2 Microstructure Visualisation

The mechanical behaviour of a material is significantly influenced by its internal structure. The Nikon SMZ800 stereo microscope equipped with a camera is used to examine the manufactured composite sandwiches' internal structure and fracture surface precisely. The stereo microscope allows examination of the samples at magnifications ranging from x20 to x120. Details about the surface characteristics and structural complexities of the samples can be identified using the stereo microscope.

2.3 Three-Point Bending Tests

To examine the relationship between mechanical behaviour and the internal structure, manufactured samples are subjected to three-point bending testing; the ASTM D790 standard is used for the testing procedure. The strain rate is selected as 0.01 min^{-1} (sometimes referred to as quasi-static). The selected strain rate is based on equipment capability and previous research at similar strain rates, ensuring comparability of the experimental data. The force is applied to all samples until the failure occurs. Three-point bending tests are performed on the Shimadzu AG-IS 50 kN universal test machine. All tests are conducted in ambient conditions to indicate the effect of room temperature. The tested specimen and test setup are shown in Figure 4.

FIGURE 4: TESTED SPECIMEN AND THREE-POINT BENDING TEST SETUP

From three-point bending tests, the flexural properties of the sample are obtained, and one of these properties is the flexural modulus. The flexural moduli of the tested samples can be determined by using the expression below:

$$E = \frac{\mathrm{F}\times l^3}{4\times \mathrm{w}\times \mathrm{b}\times h^3} \quad (1)$$

This equation depends on the dimensions of the specimen, the applied force to the specimen, and the deformation of the specimen. In this case, E represents the flexural modulus of the tested sample, F for the applied force to the specimen, l for the span between supports, w for the deflection, and b and h for the test specimen's width and height, respectively.

3. RESULTS AND DISCUSSION

In this section, the results of the three-point bending tests and images acquired from the microstructure visualisation procedure are presented, and the effects of internal structure geometry on the mechanical behaviour of the structure are discussed.

3.3 Microstructure Visualisation

The purpose of the microstructure visualisation part of this study is to examine the internal structure of the samples and gather information about their deformation behaviour by capturing images of the fracture surfaces. Internal structure and fracture surface images of the damaged samples are given in Figures 5 to 10 and presented in this section. Figures 5, 7-10 show the plane in which the force is applied, and Figure 6 shows the plane that is perpendicular to that plane.

In general, the images show that the surface roughness of the samples is at the intended level. This is due to the fact that 3D-printed parts are typically made up of many individual layers. Surface roughness has a significant role in terms of the mechanical behaviour of the sample. It is, therefore, important to consider this when designing and testing 3D-printed parts. However, the surfaces do not show any major inconsistencies or significant defects. It can, therefore, be assumed that the printing process has been successfully completed to achieve the required consistency, which would allow the effects of the internal structure to be studied.

In Figure 5, the internal structure of the Cross Square 4 sample is shown. From that figure, it can be seen that this internal structure consists of smooth square geometries, no geometric errors caused by printing in the internal structure, and the square cells are well interconnected.

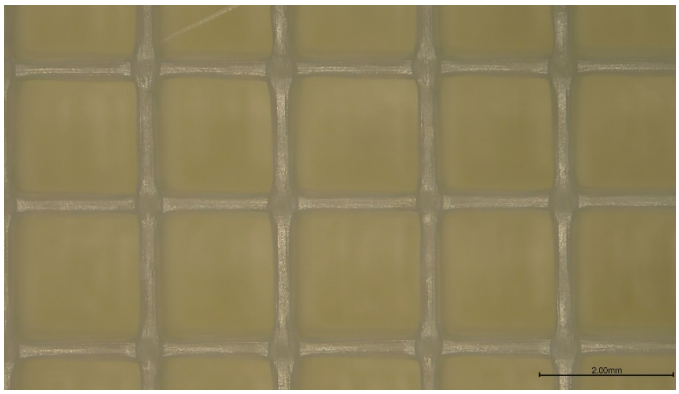

FIGURE 5: INTERNAL STRUCTURE OF CROSS SQUARE 4 SAMPLE

In Figure 6, the deformation surface of the Cross Square 2 sample is pictured. Here, no large debonding is seen, and the fracture behaviour of the material is as expected.

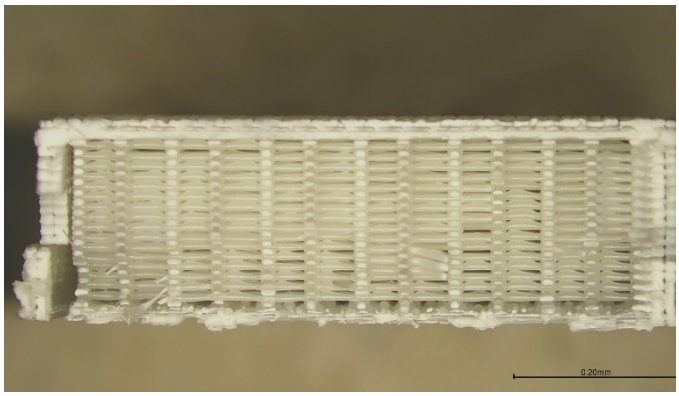

FIGURE 6: DEFORMATION SURFACE OF CROSS SQUARE 2 SAMPLE

Figures 7-9 present the inner structure visualisation of auxetic geometry samples (AUX 1, AUX 3 and AUX 4, respectively). The visual characteristics of 3D printed samples do not raise any significant concerns and reveal its auxetic structure.

In Figure 7, the internal structure of the AUX 1 sample is given. Upon comparing the representation of the design of AUX 1 in Figure 1 to the printed internal structure, no errors related to the 3D printing procedure are found. On closer inspection, the cells are found to be well bonded. There are no geometric inaccuracies.

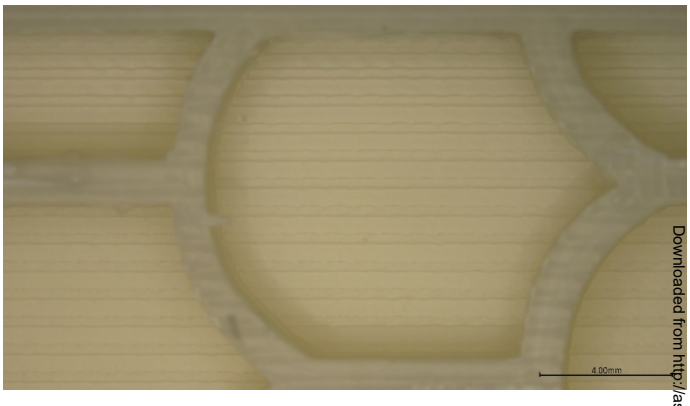

FIGURE 7: INTERNAL STRUCTURE OF AUX 1 SAMPLE

The internal structure of the AUX 3 sample is shown in Figure 8. When the representation of the design of AUX 3, which is given in Figure 1, is compared to the acquired image from the stereo microscope, it is seen that there are no errors related to the manufacturing process. Additionally, when a detailed investigation is made, cells are bonded well, with no geometric inaccuracy.

FIGURE 8: INTERNAL STRUCTURE OF AUX 3 SAMPLE

The internal structure of the AUX 4 sample is illustrated in Figure 9. When the representation of the design of AUX 4 given in Figure 1 is compared to the printed internal structure, it is seen that details that represent the AUX 4 design are reproduced, which means that the 3D printing procedure is carried out successfully. Also, when the given image is explored in detail, it is evident that the cells have good bonding.

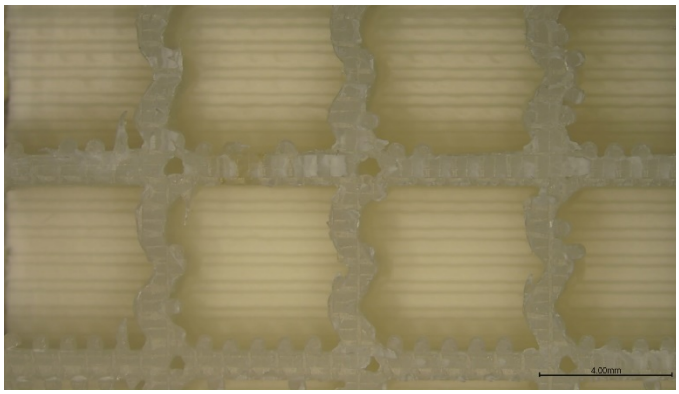

FIGURE 9: INTERNAL STRUCTURE OF AUX 4 SAMPLE

In Figure 10, the deformation surface of the AUX 3 sample is visualised. In this case, no large debonding is seen, and the fracture behaviour of the material is as expected. Although the internal structure in the images is similar to the intended internal structures, there is no printer-related error during manufacturing. Examining the relationship between the type of loading and the orientation of the auxetic structure can also be done by examining the fracture surfaces. In this case, the internal structure orientation appears as expected. No significant flaws are seen due to the manufacturing process.

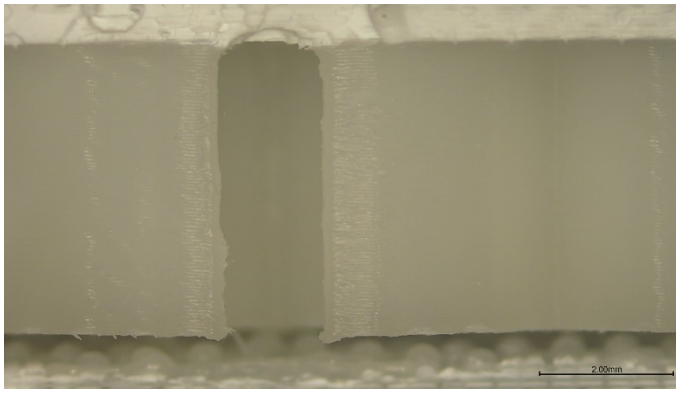

FIGURE 10: INTERNAL STRUCTURE OF AUX 3 SAMPLE

3.4 Three-Point Bending Tests

The results of the three-point bending tests aim to characterise the structure-dependent mechanics of the manufactured panels and are presented in this section. In order to emphasise the reliability of results, each test is repeated with three samples. Flexural modulus, flexural strength, and elongation at break values of each sample are conducted from three-point bending tests. The average of the results is taken and given in Tables 1 and 2.

TABLE 1: MECHANICAL PROPERTIES OF CROSS SQUARE SAMPLES

Cross Square Geometry	1	2	3	4	5
Flexural Strength (MPa)	10.0	11.6	8.4	8.5	9.6
Flexural Modulus (MPa)	132.0	155.6	93.8	103.7	117.2
Elongation at Break	0.0823	0.1096	0.1327	0.1038	0.1087

From Table 1, the change in mechanical properties of the Cross Square structures can be observed. It can be said that "Cross Square geometry 2" is the stiffest geometry due to its highest flexural modulus (155.62 MPa), and Cross Square geometry 1, 5, 4 and 3 follow, respectively.

Flexural modulus is not the only parameter when considering mechanical properties. Interpretations can be made regarding the mechanical behaviour of the structure based on elongation at break values. Elongation at break values gives information about the ductile behaviour of the material. Elongation at break values of Cross Square geometries is also given in Table 1. From Table 1, Cross Square geometry 3 has the highest elongation at break value (0.1327). Based on this result, Cross Square geometry 3 is the most ductile geometry compared to other ones.

TABLE 2: MECHANICAL PROPERTIES OF AUXETIC SAMPLES

Auxetic Geometry	1	2	3	4	5
Flexural Strength (MPa)	10.2	11.2	10.4	10.5	6.4
Flexural Modulus (MPa)	125.4	139.9	122.6	142.9	79.0
Elongation at Break	0.0968	0.1032	0.1304	0.0853	0.1267

Table 2 shows the change in mechanical properties of the auxetic structures. It can be observed that "AUX 4" has the highest flexural modulus (142.88 MPa) and is, therefore, the stiffest geometry. Following this, in descending order, are rectilinear geometries 2, 1, 3 and 5.

As previously stated, elongation at break values provides information about the ductile behaviour of the material. Table 2 shows the elongation at break values of auxetic geometries. It can be observed that AUX 3 has the highest elongation at break value (0.1304), indicating that it is the most ductile geometry compared to the others.

In order to explore the relationship between auxetic and Cross Square geometry on material behaviour, the change in flexural modulus, flexural strength and elongation at break concerning geometry is given as bar graphs in Figures 11 to 13.

The figures demonstrate that the flexural strength values of auxetic and Cross Square structures vary depending on their geometries. There is no general assumption that can be made between auxetic and Cross Square structures. Therefore, each geometry must be evaluated individually.

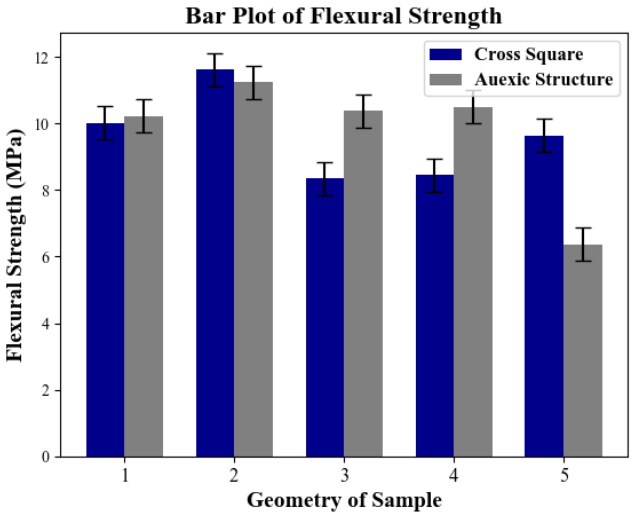

FIGURE 11: FLEXURAL STRENGTH OF THE MANUFACTURED SAMPLES CONCERNING STRUCTURAL GEOMETRY

In Figure 11, the flexural strength of each auxetic and Cross Square geometry combination is evaluated comparatively. A noticeable increase is seen in flexural strength values between auxetic and Cross Square geometries in geometry combinations 3 and 4, and in geometry combination 1, a 1.96% increase is seen. Additionally, in geometry combinations 2 and 5, flexural strength results between auxetic and Cross Square geometries tend to decrease. While the decrease in geometry combination 2 is recorded as 3.27%, in geometry combination 5, a significant decrease is noted.

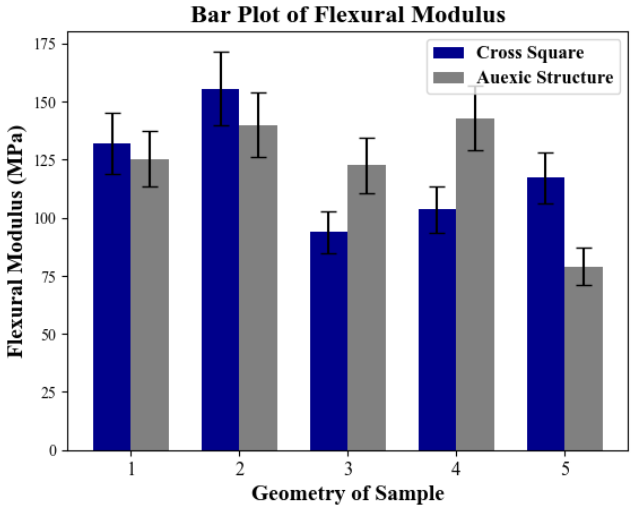

FIGURE 12: FLEXURAL MODULUS OF THE MANUFACTURED SAMPLES CONCERNING STRUCTURAL GEOMETRY

In Figure 12, the flexural modulus of each auxetic and Cross Square geometry combination is evaluated comparatively. Similar to flexural strength results, an increase between auxetic and Cross Square geometries in geometry combinations 3 and 4 and a decrease in geometry 2 and 5 are shown. Contrary to flexural strength results, a decrease in flexural modulus results is observed in geometry combination 1 from Cross Square to auxetic internal structures. While geometry combinations 1, 2, and 5 show stiffer behaviour in the Cross Square internal structure, geometry 3 and 4 show stiffer behaviour in the auxetic internal structure.

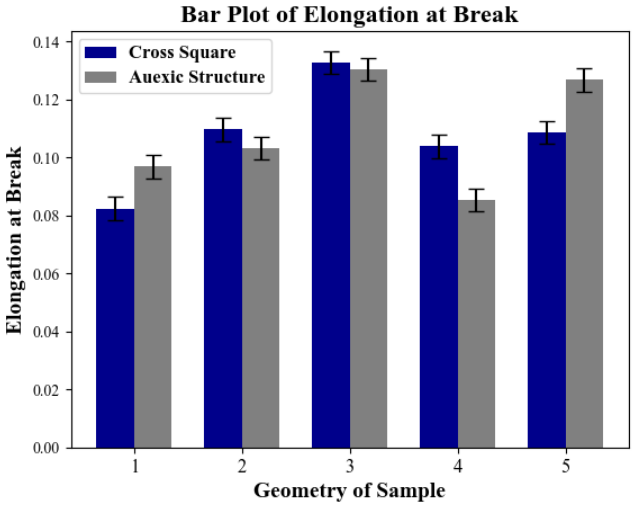

FIGURE 13: ELONGATION AT BREAK VALUES OF THE MANUFACTURED SAMPLES CONCERNING STRUCTURAL GEOMETRYs

In Figure 13, the elongation at break values of each auxetic and Cross Square geometry combination is evaluated comparatively. From the results in geometry combinations 1 and 5, auxetic samples have more ductile behaviour due to higher

elongation at break values than Cross Square structured ones. In geometry combinations 2,3 and 4, elongation at break values of Cross Square structured samples increase compared to auxetic ones and the auxetic structure 4 has the highest increase in terms of percentage.

From the three-point bending test, results are obtained as force and displacement; within the light of these data, stress-strain plots of the tested samples can be conducted. Since standard deviations and averages of the results satisfy confidence level, stress-strain plots of the one sample of each configuration are drawn. In Figures 14 and 15, the stress–strain diagrams of the manufactured samples are shown.

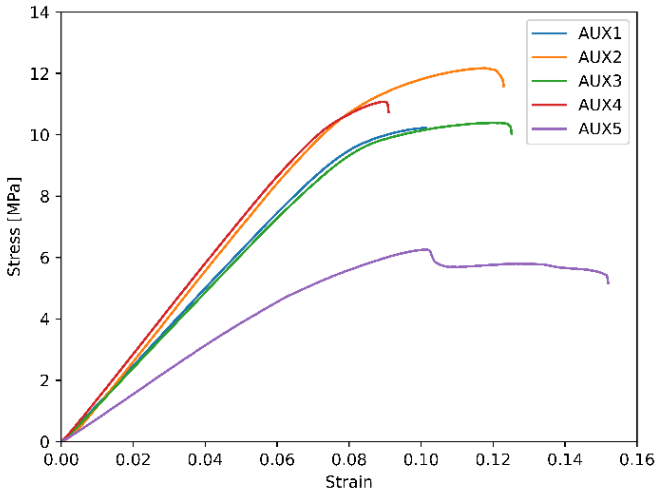

FIGURE 14: STRESS-STRAIN CURVE OF AUXETIC SAMPLES

In Figure 14, stress-strain curves of auxetic samples are compared. The curves of the samples except the AUX 5 sample show similar trends. Although the flexural modulus and flexural strength behaviours of AUX 1 and AUX 3 samples are quite similar, the difference in their mechanical behaviour is clearly evident in the elongation at break values and the time until rupture after reaching the flexural strength. AUX3 samples have a higher elongation at break values, and the line between flexural strength and failure point is longer than the AUX1 sample results. This indicates that in AUX 1 geometry failure occurs quicker than the AUX 3 samples and they show more ductile behaviour. A similar observation can be conducted for AUX 2 and AUX 4 samples. The results show that AUX 2 samples behave more ductile than AUX 4 samples, and failure of these samples occurs slowly.

Upon consideration of the AUX 5 sample, it is evident that it exhibits distinct behaviour from the other samples. Although the flexural modulus and flexural strength are lower than in other samples, and they break at earlier values compared to other samples, load bearing continues for a certain period of time after the failure occurs in AUX 5 samples. Additionally, there is no catastrophic sudden failure. This feature can be useful when the structure needs to withstand a load, even in the event of a failure, preventing immediate collapse.

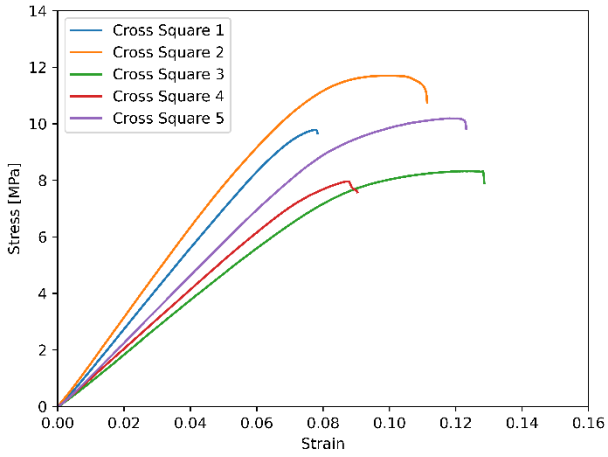

FIGURE 15: STRESS-STRAIN CURVES OF CROSS SQUARE SAMPLES

The curves in Figure 15 exhibit similar trends and flexural modulus and flexural strength behaviour evaluated in previous paragraphs. Interpretations can be made based on the elongation at break behaviour. The maximum elongation at break behaviour can also be observed graphically in the Cross Square 3 sample. In addition, when the deformation behaviour of the materials before failure is examined, it is seen that in the Cross Square 1 sample, the failure occurs rapidly after the flexural strength value is reached, whereas, in the Cross Square 2 sample, it takes a longer time for the failure to occur. The area under the stress-strain graph also provides insight into the material's toughness behaviour. Based on this information, it can be concluded that the Cross Square 5 sample (which has the highest area under the curve) is the toughest one.

4. CONCLUSION

The 3D printing process employed advanced techniques and precise parameters, ensuring the fabrication of samples with varied internal structures for a three-point bending test. The inclusion of both auxetic and non-auxetic geometries provided a robust foundation for evaluating and comparing the performance of the samples.

This study focuses on the mechanical behaviour of 3D-printed sandwich panels with different internal structures. Within the scope of this study, sandwich structures with five different internal structures are manufactured using the 3D printing method. The manufactured structures are conducted mechanical tests and visual examinations to understand the internal structure-dependent mechanical behaviour. From visual examinations, no errors in the internal structure of the manufactured panels are observed. Fracture surfaces of the manufactured samples are also explored, and no large debonding is seen, which means that the fracture behaviour of the samples is consistent with the results from the mechanical test. As a result of the experiments, it is found that each internal structure has its own characteristics. A comparative characterisation study is also

carried out to compare the Cross Square and auxetic structures. In this context, it is assessed that the most optimal internal structure selection can be made under the conditions to which the internal structure will be exposed.

Future work could expand in several directions, building on the results of this investigation of the mechanical behaviour of different infill lattice geometries in 3D printed structures. One possibility is to explore the influence of hybrid infill patterns that combine aspects of both rectilinear and honeycomb designs, potentially achieving a balance between strength and material efficiency. Furthermore, it may be possible to study the effect of variable infill densities within a single print, like functionally graded structures, to further optimise material usage and improve performance. Similarly, the progress in 3D printing technology, such as the use of multi-material printing, opens up the possibility of creating gradient infill structures where material properties vary across the print, tailoring the mechanical response to specific application needs. In addition, the use of machine learning algorithms can predict the best infill geometries, automating the design process for custom applications. This would not only enhance the current knowledge of lattice structures but also expand the capabilities of additive manufacturing in industrial and engineering applications.

ACKNOWLEDGEMENTS

The authors would like to thank the Composite Materials Laboratory in the Faculty of Mechanical Engineering of Istanbul Technical University for their contribution to this research.

REFERENCES

[1] Srivastava, A., 2015, "Elastic Metamaterials and Dynamic Homogenization: A Review," Int J Smart Nano Mater, **6**(1), pp. 41–60.

[2] Costa, J. T., Silveirinha, M. G., and Maslovski, S. I., 2009, "Finite-Difference Frequency-Domain Method for the Extraction of Effective Parameters of Metamaterials," Phys Rev B Condens Matter Mater Phys, **80**(23), pp. 1–12.

[3] Dilberoglu, U. M., Gharehpapagh, B., Yaman, U., and Dolen, M., 2017, "The Role of Additive Manufacturing in the Era of Industry 4.0," Procedia Manuf, **11**(June), pp. 545–554.

[4] Lee, C. H., Padzil, F. N. B. M., Lee, S. H., Ainun, Z. M. A., and Abdullah, L. C., 2021, "Potential for Natural Fiber Reinforcement in Pla Polymer Filaments for Fused Deposition Modeling (Fdm) Additive Manufacturing: A Review," Polymers (Basel), **13**(9), p. 1407.

[5] Marimuthu, S., Clark, D., Allen, J., Kamara, A. M., Mativenga, P., Li, L., and Scudamore, R., 2013, "Finite Element Modelling of Substrate Thermal Distortion in Direct Laser Additive Manufacture of an Aero-Engine Component," Proc Inst Mech Eng C J Mech Eng Sci, **227**(9), pp. 1987–1999.

[6] Öztekin, V., and Yılmaz, Ş., 2023, "Experimental and Numerical Investigation of the Gurson–Tveergard–Needleman Model Parameters for AISI 1045 Steel," Steel Res Int, **94**(6).

[7] Talischi, C., Paulino, G. H., and Le, C. H., 2009, "Honeycomb Wachspress Finite Elements for Structural Topology Optimization," Structural and Multidisciplinary Optimization, **37**(6), pp. 569–583.

[8] Maskery, I., and Ashcroft, I. A., 2020, "The Deformation and Elastic Anisotropy of a New Gyroid-Based Honeycomb Made by Laser Sintering," Addit Manuf, **36**, p. 101548.

[9] Plocher, J., and Panesar, A., 2020, "Effect of Density and Unit Cell Size Grading on the Stiffness and Energy Absorption of Short Fibre-Reinforced Functionally Graded Lattice Structures," Addit Manuf, **33**(March).

[10] Mukherjee, S., and Adhikari, S., 2022, "The In-Plane Mechanics of a Family of Curved 2D Lattices," Compos Struct, **280**.

[11] Mukhopadhyay, T., Adhikari, S., and Batou, A., 2019, "Frequency Domain Homogenization for the Viscoelastic Properties of Spatially Correlated Quasi-Periodic Lattices," Int J Mech Sci, **150**(September), pp. 784–806.

[12] Adhikari, S., Mukhopadhyay, T., and Liu, X., 2021, "Broadband Dynamic Elastic Moduli of Honeycomb Lattice Materials: A Generalized Analytical Approach," Mechanics of Materials, **157**(September 2018).

[13] Seharing, A., Azman, A. H., and Abdullah, S., 2020, "A Review on Integration of Lightweight Gradient Lattice Structures in Additive Manufacturing Parts," Advances in Mechanical Engineering, **12**(6), pp. 1–21.

[14] Alomar, Z., and Concli, F., 2020, "A Review of the Selective Laser Melting Lattice Structures and Their Numerical Models," Adv Eng Mater, **22**(12).

[15] Pan, Z., Ma, R., Wang, D., and Chen, A., 2018, "A Review of Lattice Type Model in Fracture Mechanics: Theory, Applications, and Perspectives," Eng Fract Mech, **190**, pp. 382–409.

[16] Li, C., Wang, F., Sun, Y., Jiang, K., Gong, S., Hu, Z., Zhou, Z., Dong, X., and Chu, J., 2018, "Lattice Dynamics, Phase Transition, and Tunable Fundamental Band Gap of Photovoltaic (K,Ba)(Ni,Nb) O3-δ Ceramics from Spectral Measurements and First-Principles Calculations," Phys Rev B, **97**(9), p. 094109.

[17] Partovi Meran, A., Toprak, T., and Muğan, A., 2014, "Numerical and Experimental Study of Crashworthiness Parameters of Honeycomb Structures," Thin-Walled Structures, **78**, pp. 87–94.

[18] Tornabene, F., and Dimitri, R., 2021, "Higher-Order Theories for Doubly Curved Laminated Lattice and Honeycomb Structures," (March).

[19] Peng, X. L., and Bargmann, S., 2021, "A Novel Hybrid-Honeycomb Structure: Enhanced Stiffness, Tunable Auxeticity and Negative Thermal Expansion," Int J Mech Sci, **190**(October), p. 106021.

[20] Schmitz, A., and Horst, P., 2014, "A Finite Element Unit-Cell Method for Homogenised Mechanical Properties of

Heterogeneous Plates," Compos Part A Appl Sci Manuf, **61**, pp. 23–32.
[21] Böhm, H. J., and Han, W., 2001, "Comparisons between Three-Dimensional and Two-Dimensional Multi-Particle Unit Cell Models for Particle Reinforced Metal Matrix Composites," Model Simul Mat Sci Eng, **9**(2), pp. 47–65.
[22] Okabe, T., Nishikawa, M., and Toyoshima, H., 2011, "A Periodic Unit-Cell Simulation of Fiber Arrangement Dependence on the Transverse Tensile Failure in Unidirectional Carbon Fiber Reinforced Composites," Int J Solids Struct, **48**(20), pp. 2948–2959.
[23] Fu, Y., and Liu, W., 2021, "Design of Mechanical Metamaterial with Controllable Stiffness Using Curved Beam Unit Cells," Compos Struct, **258**.
[24] Zeman, J., Peerlings, R. H. J., and Geers, M. G. D., 2011, "Non-Local Energetics of Random Heterogeneous Lattices," J Mech Phys Solids, **59**(6), pp. 1214–1230.
[25] Zabulionis, D., and Rimša, V., 2018, "A Lattice Model for Elastic Particulate Composites," Materials, **11**(9), pp. 1–14.
[26] Tornabene, F., Viscoti, M., Dimitri, R., and Antonietta Aiello, M., 2021, "Higher-Order Modeling of Anisogrid Composite Lattice Structures with Complex Geometries," Eng Struct, **244**(June), p. 112686.
[27] Chen, H., Jiao, Y., and Liu, Y., 2016, "A Nonlocal Lattice Particle Model for Fracture Simulation of Anisotropic Materials," Compos B Eng, **90**, pp. 141–151.
[28] Bisoi, A., Tüfekci, M., Öztekin, V., Denimal Goy, E., and Salles, L., 2023, "Experimental Investigation of Mechanical Properties of Additively Manufactured Fibre-Reinforced Composite Structures for Robotic Applications," Applied Composite Materials, (0123456789).
[29] Chacón, J. M., Caminero, M. A., Núñez, P. J., García-Plaza, E., García-Moreno, I., and Reverte, J. M., 2019, "Additive Manufacturing of Continuous Fibre Reinforced Thermoplastic Composites Using Fused Deposition Modelling: Effect of Process Parameters on Mechanical Properties," Compos Sci Technol, **181**(May), p. 107688.
[30] Ziemian, C., Sharma, M., and Ziemi, S., 2012, "Anisotropic Mechanical Properties of ABS Parts Fabricated by Fused Deposition Modelling," Mechanical Engineering.
[31] Chadha, A., Ul Haq, M. I., Raina, A., Singh, R. R., Penumarti, N. B., and Bishnoi, M. S., 2019, "Effect of Fused Deposition Modelling Process Parameters on Mechanical Properties of 3D Printed Parts," World Journal of Engineering, **16**(4), pp. 550–559.
[32] Sood, A. K., Ohdar, R. K., and Mahapatra, S. S., 2010, "Parametric Appraisal of Mechanical Property of Fused Deposition Modelling Processed Parts," Mater Des, **31**(1), pp. 287–295.
[33] Wang, K., Xie, X., Wang, J., Zhao, A., Peng, Y., and Rao, Y., 2020, "Effects of Infill Characteristics and Strain Rate on the Deformation and Failure Properties of Additively Manufactured Polyamide-Based Composite Structures," Results Phys, **18**, p. 103346.
[34] Khan, S. A., Siddiqui, B. A., Fahad, M., and Khan, M. A., 2017, "Evaluation of the Effect of Infill Pattern on Mechanical Stregnth of Additively Manufactured Specimen," Materials Science Forum, **887 MSF**, pp. 128–132.
[35] Tüfekci, M., 2023, "Performance Evaluation Analysis of Ti-6Al-4V Foam Fan Blades in Aircraft Engines: A Numerical Study," Composites Part C: Open Access, **12**(September), p. 100414.
[36] Tüfekci, M., Öztekin, V., Pir, İ., Alioğlu, M., Dikicioğlu, C., Dikicioğlu, A., and Tüfekci, E., 2023, "Low Strain Rate Mechanical Performance of Balsa Wood and Carbon Fibre-Epoxy-Balsa Sandwich Structures," Composites Part C: Open Access, **12**(November), p. 100416.
[37] Adhikari, S., 2021, "The In-Plane Mechanical Properties of Highly Compressible and Stretchable 2D Lattices," Compos Struct, **272**.
[38] Mukherjee, S., and Adhikari, S., 2021, "A General Analytical Framework for the Mechanics of Heterogeneous Hexagonal Lattices," Thin-Walled Structures, **167**.
[39] Mukherjee, S., Cajić, M., Karličić, D., and Adhikari, S., 2023, "Enhancement of Band-Gap Characteristics in Hexagonal and Re-Entrant Lattices via Curved Beams," Compos Struct, **306**.

